Numerical Modelling of Traffic on the M25 Motorway: Part I

Joanne Morgan
University of Reading
June 2001

Abstract- *A one-equation model of traffic flow is used based on a non-convex function derived from real data. The exact solutions are constructed which are used to test several numerical schemes. Results from the best of the schemes are then compared with real data.*

1 Introduction

Traffic flow can be modelled using microscopic car-following theory, macroscopic fluid dynamic based models, or combinations of both (see e.g. Daganzo [2], Nagel [9] and Helbing [3]). This paper considers the application of the Lighthill-Whitham-Richards (LWR) model of traffic flow proposed in the 1950's [8], [11] to averaged actual data gathered from the M25 motorway (supplied by the TRL/Highways agency). It describes different fitted velocity functions and compares analytic solutions to two test cases to the numerical solutions from four different numerical schemes. The paper then compares numerical solutions from the best of these schemes to the M25 data.

The model studied is based on a single carriageway with no on or off ramps, and data is averaged over all available lanes.

Section 2 describes the one-equation model, and considers a number of different fitted velocity functions. In Section 3 we derive the exact analytic solution to two test problems. Section 4 compares the numerical solutions from four different numerical schemes on the two test problems from Section 3. Then in Section 5 we compare the averaged real data from a stretch of the M25 with no on/off ramps to a numerical simulation using the most accurate scheme from Section 4. Conclusions are given in Section 5 and Section 6 suggests further work.

2 One-Equation Model

The LWR model,

$$\frac{\partial \rho}{\partial t} + \frac{\partial (\rho V(\rho))}{\partial x} = 0, \tag{1}$$

is in effect a conservation of mass equation, where ρ is used to represent the traffic density and $V(\rho)$ is the velocity associated with that density. One of the basic assumptions about this model is that the velocity is a function of density alone, and that consequently any changes in density are immediately reflected in changes in the velocity. Obviously this argument has some flaws: for example, in practice reactions to changes in density do not happen instantaneously.

The velocity $V(\rho)$ and flux $f = \rho V(\rho)$ for a given density are crucial in modelling the flow. The overall shape of the graph of $V(\rho)$ is still under debate, particularly for congested traffic flow.

There are many options for the choice of $V(\rho)$. The original choice in [13] was

$$V_1(\rho) = U_{max}\left(1 - \frac{\rho}{\rho_{max}}\right) \tag{2}$$

where U_{max} is a given maximum speed on the road (typically 140km/h) and ρ_{max} is a maximum density (typically 220 veh/km).

By considering averaged real data collected from a stretch of the M25, it was observed that the non-convex flux function,

$$V_2(\rho) = U_{max} e^{-9\rho/\rho_{max}} \tag{3}$$

captures many of the properties observed in the real data, although not all, see f_R in Fig.1 (right).

Another velocity function, similar to the one used by Kerner and Konhauser in [4], [5] and [6], is

$$V_3(\rho) = \left(\frac{a}{1 + e^{\frac{\rho - b}{c}}}\right), \tag{4}$$

where $a = 120$, $b = 0.15\rho_{max}$ and $c = 0.06\rho_{max}$ are good choices for approximating the observed data.

Fig. 1 (left) shows the three velocity functions (V_1, V_2, V_3) plotted against ρ, compared to the real velocity data V_R, and Fig.1 (right) shows the corresponding flux functions, (f_1, f_2, f_3) plotted against ρ, compared to the real

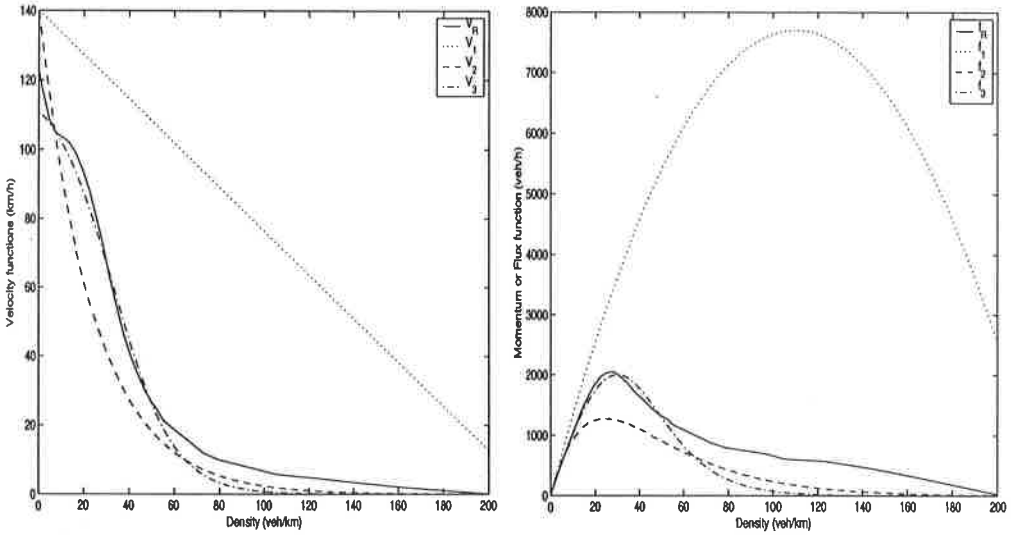

Figure 1: V_R is the real averaged data, V_1, V_2 and V_3 are velocity functions (left). f_R is the real data averaged for the momentum (ρv), and f_1, f_2 and f_3 are the flux functions (right).

flux data f_R (right). The flux graph is often referred to as the *Fundamental Diagram.*

To process the real data, we calculated the average velocity and flux for the given densities as follows. Since we are considering averaged behaviour along the whole stretch of road to get the typical values, data was considered at each post, for each lane. The data was collected over a week as an average velocity (km/h) over a minute period for each lane, together with a count of the number of cars passing each post in each lane during that minute, (veh/min). The density at each post for each minute interval was calulated using the equation

$$density = \frac{count * 60}{velocity}.$$

The densities, and corresponding velocities, were sorted and grouped into small intervals of density. Mean velocities and densities were then calculated for each interval, (V_R, ρ_R). The average flux, f_R, is then calculated from

$$f_R = \rho_R * V_R.$$

It can be seen that f_3 follows the real data well for small ρ, but for large ρ there is no good match.

3 Test Problems

To test the different schemes considered later in the paper, these were compared with exact solutions. Here the densities and velocity functions were normalised to simplify the calculations.

1. Square Wave

   The first test case is a square wave of height 1/2 with zero density outside of the wave, Fig.2. The left side of the wave was positioned at a distance of 10 unit lengths from the left hand end of the road, and the right side of the wave positioned at 20 unit lengths. Hence

$$\rho(x,0) = \begin{cases} \frac{1}{2} & 10 \leq x \leq 20 \\ 0 & otherwise. \end{cases} \tag{5}$$

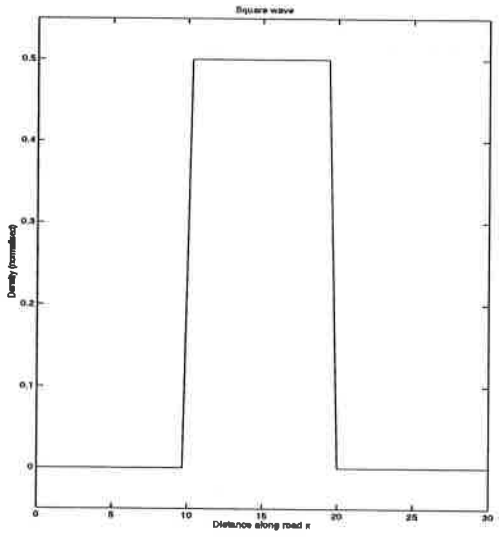

Figure 2: Test problem 1.

2. Half-Cosine Wave

The second test case is a half cosine wave joined to a discontinuity, Fig.3. Again, the density outside of the perturbation was zero. Here

$$\rho(x,0) = \begin{cases} \frac{1}{2}cos^2\left(\frac{\pi x}{20}\right) & 10 \leq x \leq 20 \\ \\ 0 & otherwise \end{cases} \tag{6}$$

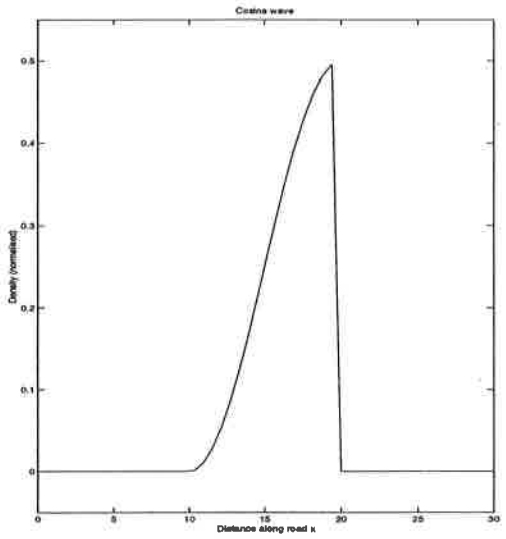

Figure 3: Test problem 2.

Analytic solutions

The exact solutions are obtained using the method of characteristics. Using equation (1) with velocity function (3), normalised, i.e.

$$V(\rho) = e^{-9\rho}, \tag{7}$$

so that

$$f(\rho) = \rho e^{-9\rho} \tag{8}$$

we have from

$$\frac{\partial \rho}{\partial t} + \frac{\partial f(\rho)}{\partial x} = \frac{\partial \rho}{\partial t} + a(\rho)\frac{\partial \rho}{\partial x} = 0 \tag{9}$$

that

$$a(\rho) = \frac{df}{d\rho} = (1 - 9\rho)e^{-9\rho}. \tag{10}$$

Now, using the chain rule, we know that

$$\frac{d\rho}{dt} = \frac{\partial \rho}{\partial x}\frac{dx}{dt} + \frac{\partial \rho}{\partial t}.$$

So that substituting $\frac{\partial \rho}{\partial t}$ in (9), we have

$$\frac{d\rho}{dt} - \frac{\partial \rho}{\partial x}\frac{dx}{dt} + a(\rho)\frac{\partial \rho}{\partial x} = 0,$$

giving

$$\frac{d\rho}{dt} - \frac{\partial \rho}{\partial x}\left(\frac{dx}{dt} - a(\rho)\right) = 0.$$

Therefore, $\frac{d\rho}{dt} = 0$ on the lines

$$\frac{dx}{dt} = a(\rho), \tag{11}$$

which implies that ρ and hence $a(\rho)$ is constant along these lines. These are the characteristics, which are straight lines in this case given by

$$x = at + x_0, \tag{12}$$

or

$$t = \frac{x - x_0}{a}, \tag{13}$$

where x_0 is the value of x at $t = 0$, and

$$a = (1 - 9\rho(x_0, 0))e^{-9\rho(x_0,0)} \tag{14}$$

from (10).

To obtain the exact solution at (x, t), we trace the characteristic that passes through that point back to the initial density profile, where ρ has the same value on that characteristic, i.e.

$$\rho(x, t) = \rho(x_0, 0) = \rho_0.$$

When characteristics cross, however, the solution becomes multiply defined and the continuous theory breaks down. This is encountered immediately when considering the square wave (5) at $x = 10$ (see Fig.5). A shock is formed moving with speed

$$\begin{aligned} s &= \frac{[f]}{[\rho]} = \frac{f_r - f_l}{\rho_r - \rho_l} \\ &= \frac{1/2e^{-9/2} - 0}{1/2 - 0} = e^{-9/2}, \end{aligned} \tag{15}$$

using the Rankine-Hugoniot jump condition [7]. The fact that it is a shock is confirmed by checking the entropy condition, due to Oleinik (see [7]), where indeed

$$\frac{f(\rho_r) - f(\rho)}{\rho_r - \rho} \leq s \leq \frac{f(\rho_l) - f(\rho)}{\rho_l - \rho}, \tag{16}$$

is satisfied $\forall \rho$.

For the discontinuity at $x = 20$ we have a different scenario. The characteristics to the left of the discontinuity have negative slope ($= -2/3e^{4/2}$), whereas to the right the characteristics have positive slope ($= 1$). Therefore these characteristics do not cross, (16) is not satisfied, and hence there is no single shock connecting these states. With the non-convex flux function, however, there is a point of inflection. In this instance if ρ_l and ρ_r are both to the left or right of the point of inflection, then the *void* created between the characteristics is *filled in* with an expansion fan. In other words, if the convex hull of the flux function is the same as the flux function itself between ρ_l and ρ_r, then the solution is purely an expansion fan. We therefore need to check where ρ_l and ρ_r are relative to the point of inflection.

The point of inflection of the flux function (8) is at $\rho = \rho_I$, where

$$f''(\rho_I) = (81\rho_I - 18)e^{-9\rho_I} = 0,$$

hence,

$$\rho_I = \frac{2}{9}. \tag{17}$$

Since at $x = 20$ $\rho_r < \frac{2}{9} < \rho_l$, ρ_l and ρ_r are on opposite sides of the point of inflection, the flux function and its convex hull are not the same. The discontinuity therefore comprises of a shock and an expansion fan, separated at ρ_T, the point where the tangent to the flux function passes through (ρ_l, f_l), see Fig.4. This ensures that we have the correct entropy-satisfying weak solution ([7]).

surprising, as Fig.1 (right) shows that f_3 mimics the average real data most closely at lower densities, whereas f_2 is closest at higher densities.

Fig.9 (right) shows the Second Order scheme with the flux limiter, using the flux function f_2 against the real averaged data over a periond of five minutes. Even thought this is the best scheme with the best fitted flux function, the results are not particularly good. The height of the peak doesn't match, and as time progresses its position no longer corresponds to the peak in the real data.

It is likely that a flux function that fits the real data more closely will perform better. This could achieved by splitting the flux function into two sections, one for congested flow and one for freeflow traffic. However the limitations of the model could be at fault.

6 Conclusions

We have considered the one-equation LWR model, and compared different possible flux functions to some real averaged data from the M25 motorway. We devised some exact solutions to two test cases for one of the non-convex flux functions, and tested some schemes against these. We took the best of these schemes and tested the model against M25 data for the different flux functions.

The test cases showed the complex nature of solutions when dealing with a non-convex flux function. For example, a discontinuity may consist of a combination of shocks and expansion fans, depending on the relative values of the ρ_l and ρ_r, to any points of inflection of the flux function. The Second Order scheme gave the most accurate results with the test cases. The real data showed the performance of the different flux functions, with accuracy varying between the functions according to levels of traffic. The best scheme with the most accurate flux function still gave unsatisfactory results even for short time simulations. It is therefore clear that a more sophisticated model is required.

7 Further Work

As mentioned before, a better fit to the real data for the flux function may produce more accurate simulations. This may be achieved by splitting the flux function into two (or more) sections, having one fit for freeflow and one for congested flow, the join between the two being continuous and differentiable.

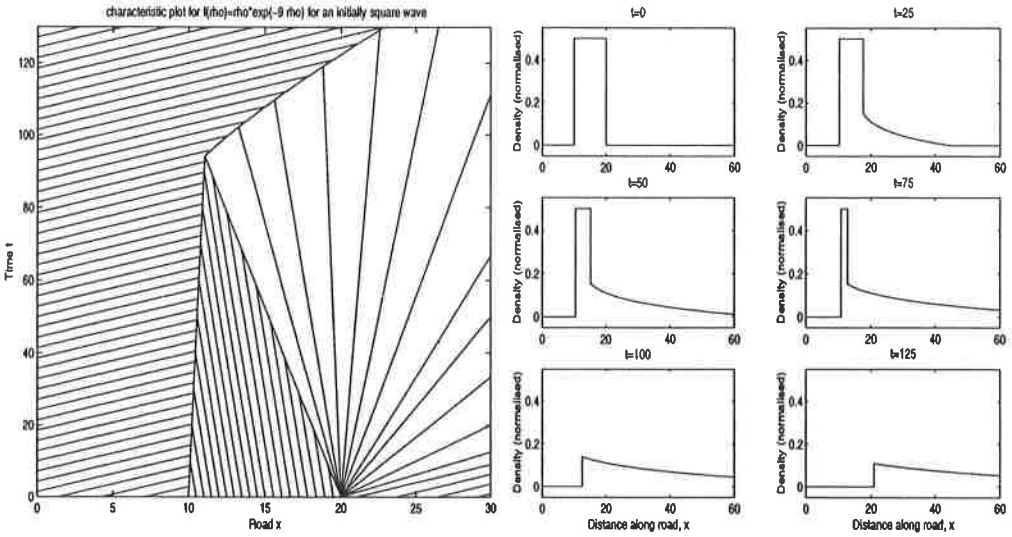

Figure 5: Characteristic diagram for test problem 1 (left). Exact solution of density along road for test problem 1 (right).

$$s = \frac{f_T - f_l}{\rho_T - \rho_l} = (1 - 9\rho_T)e^{-9\rho_T},$$

and since ρ_l is unchanged while the shock is moving, ρ_T is constant, and thus so is the speed until the shocks collide (Fig.5).

To calculate the expansion fan to the right of the shock, between ρ_T and $\rho_r = 0$, given (x, t) we find the slope of the characteristic, $1/A$, (where $f'(\rho_T) \leq A \leq f'(\rho_r)$) from (13), i.e.

$$A = \frac{x - 20}{t}. \tag{23}$$

Using A we can again find ρ using Newton iteration, from

$$f'(\rho) = (1 - 9\rho)e^{-9\rho} = A,$$

$$F = (1 - 9\rho)e^{-9\rho} - A,$$

$$\frac{dF}{d\rho} = (81\rho - 18)e^{-9\rho}. \tag{24}$$

The density ρ can then be found using (22).

When the shocks meet, we are, in the first instance, left with a discontinuity of height ρ_T followed by an expansion fan (Fig.5 left). This new discontinuity is a shock whose speed can be calculated using (15), where $\rho_l = 0$ and ρ_r is given by ρ_T. The shock therefore moves with positive speed and hence, as it moves, its height decreases, thus changing the shock speed. The shock path will therefore no longer be a straight line in the characteristic diagram. The shape of the shock can be calculated numerically using Euler's method. Starting at the initial position of the colliding shocks, we calculate the instantaneous shock speed, and using that, move a distance δx in time δt. This new position (x, t) crosses a characteristic from the expansion fan, so A can be calculated using (23), as can the new ρ_r, (24), and hence the new shock speed (15). This is then repeated as far as is required. The resulting density profile will be a shock moving with positive but decreasing speed, with decreasing height, followed by an expansion fan of increasing width (see Fig.5 (right)).

The second test case, (6), can be treated similarly. The discontinuity is of the same form, and has the same properties as for the square wave, i.e. a shock from $\rho_l = 1/2$ to ρ_T, and an expansion fan from ρ_T to $\rho_r = 0$. The shock moves with constant negative speed, while the width of the expansion fan increases with time. The wave speeds, a, of the curved section (between $x = 10$ and $x = 20$) vary from $a = 1$, decreasing to a minimum of $2/9e^{-2}$ when $f''(\rho) = 0$, (17), then increasing again to $f'(\rho_r) = -7/2e^{-9/2}$.

Since the slopes of the characteristics vary in this way, inevitably there will be a point where some cross, and hence form a shock. To find the position of the initial shock formation it is necessary to look at the *characteristic envelope* to determine when two neighbouring characteristics first cross, that is have the same x value for a given time, t. To do this, we look at where a small change in the initial position x_0, produces no change in x, i.e.

$$\frac{dx}{dx_0} = 0. \tag{25}$$

Since x is given by (12), i.e.

$$x = at + x_0,$$

a is as in (14) and

$$\rho_0 = \rho(x_0, 0) = \frac{1}{2} cos^2 \left(\frac{\pi x_0}{20} \right),$$

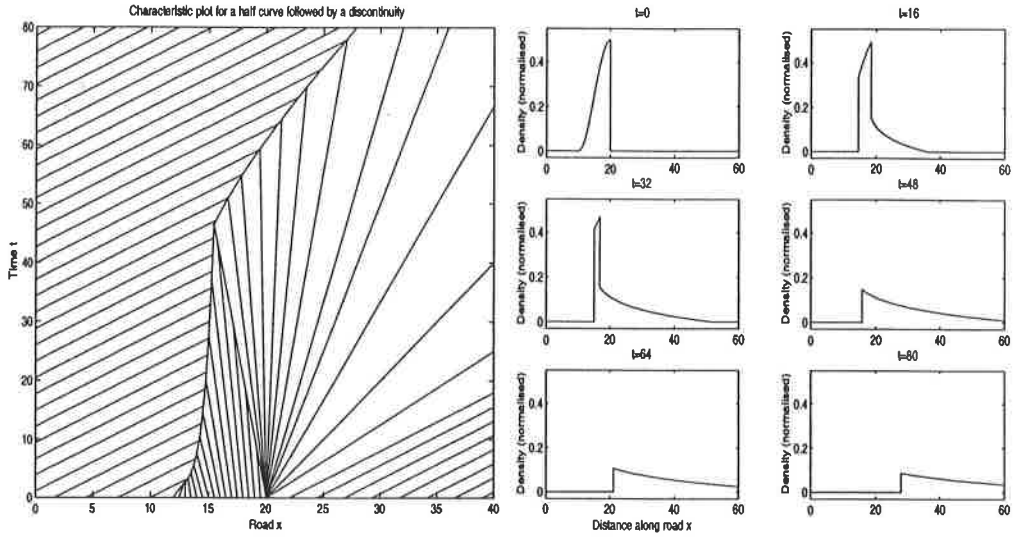

Figure 6: Characteristic diagram for test problem 2 (left). Exact solution of density along road for test problem 2 (right).

for $10 \leq x_0 \leq 20$.

Differentiating x w.r.t. x_0 gives

$$\frac{dx}{dx_0} = \frac{da}{dx_0}t + 1, \tag{26}$$

where

$$\frac{da}{dx_0} = \frac{da}{d\rho_0}\frac{d\rho_0}{dx_0} = \left((81\rho_0 - 18)e^{-9\rho_0}\right)\left(-\frac{\pi}{40}sin\left(\frac{\pi x_0}{10}\right)\right).$$

Hence, $\frac{dx}{dx_0} = 0$ when

$$t = -\left(\frac{da}{dx_0}\right)^{-1}.$$

To find the first time that the characteristics cross, we seek the minimum value of t that makes (25) true, i.e. where $\frac{dt}{dx_0} = 0$ (and $\frac{d^2t}{dx_0^2} > 0$). This happens when $x_0 = 11.643$, i.e. for $(x, t) = (12.830, 2.251)$. We can therefore construct the full characteristic diagram (Fig.6 (left)).

4 Schemes

Since equation (1) is in conservation form, where ρ is the conserved variable, a number of conservative numerical schemes can be applied to it. By choosing the velocity function V_2 of (3) and considering initial conditions (5) or (6), results can be compared to the analytic solution (Fig.(7) and Fig(8)). The numerical schemes considered here are

- First Order Upwind with an Entropy Fix ([7])
- Second Order with a Flux Limiter (Minmod)
- Engquist-Osher
- Lax-Friedrichs

4.1 First Order Upwind

This scheme subtracts $\nu_{j-\frac{1}{2}}\Delta\rho_{j-\frac{1}{2}}$ from either the left or right node, depending on the wave direction, where $\Delta\rho_{j-\frac{1}{2}} = \rho_j - \rho_{j-1}$, and where $\nu_{j+\frac{1}{2}}$ is defined by

$$\nu_{j+\frac{1}{2}} = \frac{\Delta t}{\Delta x}\left[\frac{f\left(\rho^n_{j+1}\right) - f\left(\rho^n_j\right)}{\rho^n_{j+1} - \rho^n_j}\right]. \tag{27}$$

This is the Courant number, which is $\frac{\Delta t}{\Delta x}\times$ *wave speed.*

To start with, set $\rho^{n+1}_j = \rho^n_j \ \forall j$.

If $\nu_{j-\frac{1}{2}} > 0$ then

$$\rho^{n+1}_j \rightarrow \rho^{n+1}_j - \nu_{j-\frac{1}{2}}\Delta\rho_{j-\frac{1}{2}}$$

else $\nu_{j-\frac{1}{2}} < 0$ and

$$\rho^{n+1}_{j-1} \rightarrow \rho^{n+1}_{j-1} - \nu_{j-\frac{1}{2}}\Delta\rho_{j-\frac{1}{2}},$$

noting here that if $\nu_{j-\frac{1}{2}} = 0$, then the wave speed is zero, and the density does not move.

4.2 First Order Upwind with an Entropy Fix

A problem with applying the First Order Upwind scheme to an entropy violating discontinuity across the sonic point ρ_s is that with a non-linear flux function the scheme may calculate the overall flux in the cell to be zero, hence the numerical solution gives a shock. In the case of a convex/concave flux function, the discontinuity should be an expansion fan. To overcome this a sonic entropy fix is required. For a convex/concave flux function, an intermediate non-physical point (ρ_m, f_m) which is the intersection of the tangents at ρ_r and ρ_l is found.

For a non-convex flux function however, the intermediate point is the intersection of the tangent at ρ_r and the tangent that forms the convex hull of $f(\rho)$ from ρ_l (see Fig.4), where ρ_T is found as before (18)-(22). The point (ρ_m, f_m) is then found by equating the derivative of f to the equation of the slope of a line for the two tangents, i.e.

$$f'(\rho_r) = \frac{f_r - f_m}{\rho_r - \rho_m}, \tag{28}$$

and

$$f'(\rho_T) = \frac{f_m - f_T}{\rho_m - \rho_T}. \tag{29}$$

Eliminating ρ_m from (28) and (29) we have that

$$f_m = f_T + f'(\rho_T)\left(\frac{f'(\rho_r) - \hat{a}}{f'(\rho_r) - f'(\rho_T)}\right)(\rho_r - \rho_T), \tag{30}$$

where

$$\hat{a} = \frac{f_r - f_T}{\rho_r - \rho_T}.$$

The First Order Upwind with the Entropy Fix is then implemented by updating the affected nodes, i.e. all points that satisfy $\rho_r < \rho_s < \rho_l$ in this case, with

$$\rho_l^{n+1} = \rho_l^n - \frac{\Delta t}{\Delta x}(f_m - f_l)$$

$$\rho_r^{n+1} = \rho_r^n - \frac{\Delta t}{\Delta x}(f_r - f_m)$$

We can find ρ_m by substituting f_m back into (28) or (29). Once (ρ_m, f_m) is found, the single discontinuity is treated as two separate discontinuities

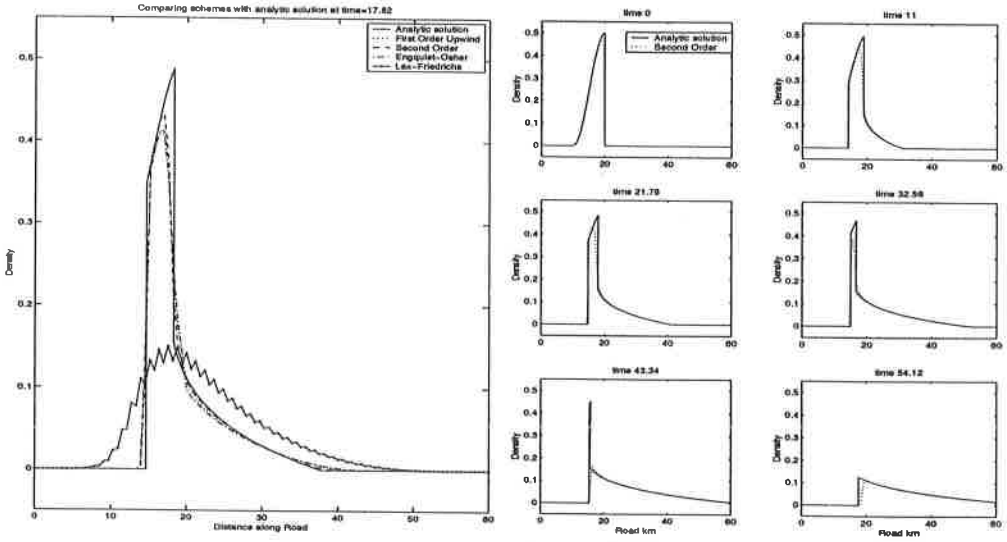

Figure 8: Comparison of 4 different schemes at a given time for test problem 2 (the half cosine wave) (left). Comparison of Second Order with Minmod to the analytic solution for test problem 2 at different times (right).

test problem of the half cosine wave compared to the four above schemes, and (right) shows the analytic solution compared to Second Order with Minmod at different times.

As expected, the second order scheme produced the best results. First Order Upwind with Entropy Fix and Engquist-Osher both gave the correct behaviour, but Lax-Friedrichs displayed too much diffusion, causing it to lose much of the shape definition.

5 Real Data

After considering the behaviour of the schemes on the test problems with artificial initial conditions, we now see how the models cope with reality. The real data we are using was collected from a section of the M25 motorway during July 1999, between junctions 10 and 15. Along that section there are a number of junctions, or on/off ramps, where the number of lanes in the road changes. To convert the data into a form that is suitable to use as initial conditions for our model, we therefore averaged the data for the four lanes giving us an *average single lane*. For this average single lane we calculated the average velocity, $\bar{v}$, and average density, $\bar{\rho}$, using

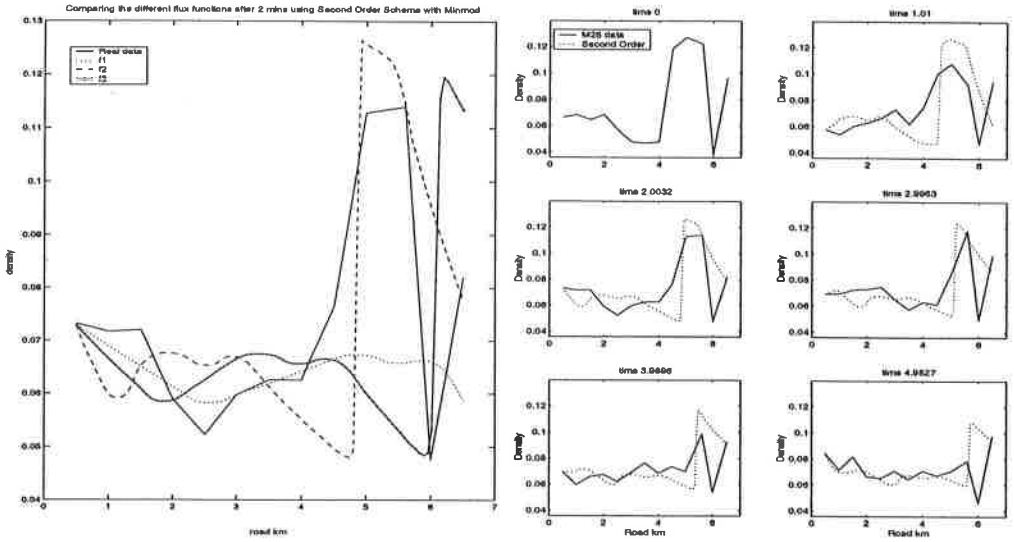

Figure 9: Comparison of 3 different flux functions at a given time, using real data from the M25 09:30 on the 15/07/99. Simulation was run using Second Order scheme with Minmod, and snapshots were taken after 2 mins (right). Second Order scheme with Minmod using f_2 with M25 data from 09:30 15/07/99 for 5 mins (left).

$$\bar{\rho} = \frac{1}{n}\left(\sum_{i=1}^{n} \frac{count_i * 60}{velocity_i}\right), \tag{37}$$

where n is the number of lanes and $velocity_i \neq 0$. When $velocity_i = 0$, one expects that $count_j = 0$ also, hence a zero value for $\frac{count_j}{velocity_j}$ is assumed. For the boundary data, when required, the real data averages were used and linearly interpolated between the minute intervals to accommodate the small time step sizes. This was done at both ends of the stretch of road, but only used when the wave direction required boundary data.

$$\bar{v} = \frac{\sum_{i=1}^{n} velocity_i * count_i}{\sum_{j=1}^{n} count_j}, \tag{38}$$

The Second Order scheme with the Minmod flux limiter was applied using the three different flux functions (f_1, f_2, f_3), of section 2, and the results are plotted against the real averaged data in Fig.9 (left). The function f_2 seems to capture the position of the highest peak most accurately, whereas f_3 appears to do slightly better at lower densities. This is perhaps not

surprising, as Fig.1 (right) shows that f_3 mimics the average real data most closely at lower densities, whereas f_2 is closest at higher densities.

Fig.9 (right) shows the Second Order scheme with the flux limiter, using the flux function f_2 against the real averaged data over a periond of five minutes. Even thought this is the best scheme with the best fitted flux function, the results are not particularly good. The height of the peak doesn't match, and as time progresses its position no longer corresponds to the peak in the real data.

It is likely that a flux function that fits the real data more closely will perform better. This could achieved by splitting the flux function into two sections, one for congested flow and one for freeflow traffic. However the limitations of the model could be at fault.

6 Conclusions

We have considered the one-equation LWR model, and compared different possible flux functions to some real averaged data from the M25 motorway. We devised some exact solutions to two test cases for one of the non-convex flux functions, and tested some schemes against these. We took the best of these schemes and tested the model against M25 data for the different flux functions.

The test cases showed the complex nature of solutions when dealing with a non-convex flux function. For example, a discontinuity may consist of a combination of shocks and expansion fans, depending on the relative values of the ρ_l and ρ_r, to any points of inflection of the flux function. The Second Order scheme gave the most accurate results with the test cases. The real data showed the performance of the different flux functions, with accuracy varying between the functions according to levels of traffic. The best scheme with the most accurate flux function still gave unsatisfactory results even for short time simulations. It is therefore clear that a more sophisticated model is required.

7 Further Work

As mentioned before, a better fit to the real data for the flux function may produce more accurate simulations. This may be achieved by splitting the flux function into two (or more) sections, having one fit for freeflow and one for congested flow, the join between the two being continuous and differentiable.

Application of high order schemes to two-equation models, e.g. Payne-Whitham [10], [13] and Aw-Rascle [1], and comparisons with M25 data will be considered in a second report.

Aknowledgements

This research is supported by the E.P.S.R.C. and supervised by Prof. Mike Baines and Dr. Pete Sweby from the University of Reading. I would also like to thank Jo White from TRL for useful discussions and the Highways Agency, in particular Brian Harbord from TSS Division, for the traffic data analysed in this report.

References

[1] A.Aw and M.Rascle. *Resurrection of 'second order' models of traffic flow?* SIAM J. Appl. Math., 60, pp916-938 (2000)

[2] C.Daganzo. *Requiem for second-order fluid approximations of traffic flow.* Transpn. Res.-B 29B, pp277-286 (1995)

[3] D.Helbing. *Gas-kinetic derivation of Navier-Stokes-like traffic equations* Phys Rev E, 53, pp 2366-2381 (1996).

[4] B.S.Kerner and P.Konhäuser. *Cluster effects in initially homogeneous traffic flow.* Phys Rev E, 48, pp R2335-R2338 (1993).

[5] B.S.Kerner and P.Konhäuser. *Structure and parameters of clusters in traffic flow.* Phys Rev E, 50, pp 54-83 (1994).

[6] B.S.Kerner, P.Konhäuser, and M.Schilke. *Deterministic spontaneous appearance of traffic jams in slightly inhomogeneous traffic flow.* Phys Rev E, 51, pp 6243-6246 (1995).

[7] R.J.LeVeque. *Numerical Methods for Conservation Laws.* Birkhäuser (1992)

[8] M.J.Lighthill and J.B.Whitham. *On kinematic waves. I:Flow movement in long rivers. II:A Theory of traffic flow on long crowded roads.* Proc. Royal Soc., A229, pp281-345 (1955)

[9] K.Nagel. *Particle hopping models and traffic flow theory.* Phys Rev E, 53, pp 4655-4672 (1986)

[10] H.J.Payne. *Models of freeway traffic and control.* Math.Models Publ. Sys.Simul. Council Proc.,28, pp 51-61 (1971).

[11] P.I.Richards. *Shockwaves on the highway.* Operations Research, 4, pp42-51 (1956)

[12] P.K.Sweby. *High Resolution Schemes Using Flux Limiters For Hyperbolic Conservation Laws.* SIAM J. Numer. Anal. 21, pp 995-1011 (1984).

[13] G.B.Whitham. *Linear and Nonlinear Waves.* John Wiley, New York, (1974).